Available online at www.sciencedirect.com
SCIENCE DIRECT®
PERGAMON
International Journal of Heat and Mass Transfer 46 (2003) 3349–3363
International Journal of HEAT and MASS TRANSFER
www.elsevier.com/locate/ijhmt

Condensation in horizontal tubes, part 1: two-phase flow pattern map

J. El Hajal [a], J.R. Thome [a,*], A. Cavallini [a,b]

[a] *Laboratory of Heat and Mass Transfer, Faculty of Engineering Science, Swiss Federal Institute of Technology, Lausanne CH-1015, Switzerland*

[b] *Dipartimento di Fisica Tecnica, University of Padova, Padova I-31531, Italy*

Received 24 June 2002

Abstract

A new flow pattern map and flow pattern based heat transfer model for condensation inside horizontal plain tubes are proposed in this two-part paper. In Part I, a new version of a two-phase flow pattern map, originally developed by Kattan et al. [J. Heat Transfer 120 (1998) 140] for flow boiling, is presented for condensation inside horizontal tubes while a new heat transfer model is presented in Part II. The new flow pattern map incorporates a newly defined logarithmic mean void fraction (LMε) method for calculation of vapor void fractions spanning from low pressures up to pressures near the critical point. Several other modifications are also made that are appropriate for condensation as opposed to evaporation. In the absence of void fraction data at high reduced pressures for these conditions, the new LMε method has been indirectly validated using the convective condensation model for annular flow and corresponding heat transfer test data at reduced pressures up to 0.8. The new map has also been successfully compared to some recent flow pattern observations for condensation and other existing flow transition criteria and maps.
© 2003 Elsevier Science Ltd. All rights reserved.

1. Introduction

Kattan et al. [1–3] proposed the first comprehensive flow boiling model for *evaporation* inside horizontal tubes based on the local flow pattern and a newly developed diabatic flow pattern map. Their new approach resulted in very significant improvements in the accuracy and reliability of heat transfer predictions compared to previous methods. As a consequence, several new condensation heat transfer models based on local flow pattern have been proposed since then by Shao and Granryd [4] and Cavallini et al. [5]. Our ultimate (but not present) objective is to arrive at a *unified approach* for modeling of flow patterns, void fractions, heat transfer coefficients and pressure drops during evaporation and condensation within horizontal tubes, and therefore a new version of the two-phase flow pattern map originally developed by Kattan et al. [1] for flow boiling is proposed here for condensation inside horizontal tubes (Part I) and a new condensation heat transfer model based on this map is presented (Part II), the latter which retains basic features of the evaporation model. In response to the high reduced pressures of interest for condensation and because of the sensitivity of flow pattern transitions, heat transfer coefficients and pressure drops to void fraction, a new log-mean method for predicting void fractions for pressures ranging from atmospheric up to near the critical pressure is also proposed.

2. Flow pattern maps for condensation

Numerous flow pattern maps have been proposed over the years for predicting two-phase flow regime

* Corresponding author. Tel.: +41-21-693-5981; fax: +41-21-693-5960.

E-mail addresses: jean.elhajal@epfl.ch (J. El Hajal), john.thome@epfl.ch (J.R. Thome), alcav@unipd.it (A. Cavallini).

0017-9310/03/$ - see front matter © 2003 Elsevier Science Ltd. All rights reserved.
doi:10.1016/S0017-9310(03)00139-X

Nomenclature

A	cross-sectional area of flow channel, m^2
A_L	cross-sectional area occupied by liquid, m^2
A_{Ld}	dimensionless liquid cross-sectional area
A_V	cross-sectional area occupied by vapor, m^2
A_{Ld}	dimensionless vapor cross-sectional area
c	empirical constant
d	tube diameter, m
$F_1(q)$	non-dimensional exponent
$F_2(q)$	non-dimensional exponent
Fr	Froude number
g	acceleration of gravity, m/s^2
G	total mass velocity of liquid and vapor, kg/(m^2 s)
G_{bubbly}	bubbly flow transition mass velocity, kg/(m^2 s)
G_{mist}	mist flow transition mass velocity, kg/(m^2 s)
G_{strat}	stratified flow transition mass velocity, kg/(m^2 s)
G_{wavy}	wavy flow transition mass velocity, kg/(m^2 s)
h_L	liquid height, m
h_{Ld}	dimensionless liquid height
h_{LV}	latent heat of vaporization, J/kg
n	empirical exponent
p_{crit}	critical pressure, N/m^2
p_r	reduced pressure
p_{sat}	saturation pressure, N/m^2
P_i	perimeter of liquid–vapor interface, m
P_{id}	dimensionless perimeter of interface, m
P_L	wetted perimeter, m
P_V	dry perimeter, m
q	heat flux, W/m^2
q_{crit}	critical heat flux, W/m^2
R	radius of tube, m
Pr_L	liquid Prandtl number
Re_L	liquid Reynolds number
T_{sat}	saturation temperature, K
ΔT_{sat}	wall-to-saturation temperature difference, K
We	Weber number
x	vapor quality
x_{IA}	intermittent to annular flow transition quality
X_{tt}	Martinelli parameter

Greek symbols

α_c	convective condensation coefficient, W/(m^2K)
δ	liquid film thickness, m
ε	vapor void fraction
λ_L	liquid thermal conductivity, W/(mK)
μ	dynamic viscosity, Ns/m^2
θ_{strat}	stratified angle, rad
ρ	density, kg/m^3
σ	surface tension, N/m
ξ	factor

Subscripts

crit	critical
d	dimensionless
h	homogeneous
L	liquid
mean	mean
min	minimum
ra	Rouhani–Axelsson
V	vapor

transitions in horizontal tubes under *adiabatic* conditions. The maps of Taitel and Dukler [6] and Baker [7] are perhaps those most quoted. Some other maps are those of Hashizume [8] and Steiner [9]. Specifically for condensation, flow pattern maps have been proposed by Breber et al. [10], by Tandon et al. [11] and recently by Cavallini et al. [5]. In addition, numerous methods have been proposed to differentiate between stratified and non-stratified condensation, such as those by Ackers and Rosson [12], Sardesai et al. [13], Shah [14] and Dobson and Chato [15]. The justification to propose a new map here is to take advantage of the new flow pattern map recently proposed by Kattan et al. [1] for adiabatic and evaporating flows in horizontal tubes and now backed by over 1000 flow pattern observations for seven different refrigerants (ammonia, R-123, R-134a, R-502, R-402A, R-404A and R-407C). Secondly, it is our long term goal to arrive at a *unified flow pattern map* for modeling heat transfer and pressure drops during evaporation, condensation and adiabatic flows within horizontal tubes but with specific adjustments for the type of flow.

3. Void fraction models

Numerous void fraction models exist for predicting the cross-sectional void fraction of a vapor in two-phase flow in a tube, which is defined as the cross-sectional area occupied by the vapor with respect to the total cross-sectional area of the flow channel. Void fraction prediction methods may be classified as follows:

- Homogeneous model (assumes the two phases travel at same velocity);
- One-dimensional models (they minimize some parameter, such as momentum or kinetic energy);
- Drift flux models (they account for the radial velocity distribution in the two phases);

- Models for specific flow regimes;
- Empirical methods.

The homogeneous model is applicable to flows where the vapor and liquid phases travel at nearly the same velocity, such as near the critical point or at very high mass velocities where the flow regime is either bubbly flow or mist flow. Other well-known methods are those of Zivi [16], Chisholm [17] and the various drift flux models. Drift flux models are particularly attractive because they account for the velocity distributions in the vapor and liquid phases and hence include the effect of mass velocity on void fraction, which the other methods do not. Notably, none of these methods is valid over the entire pressure range up to the critical pressure since none tend to the homogeneous model as $p_{sat} \rightarrow p_{crit}$.

4. Cavallini condensation heat transfer database

In the absence of void fraction data at high reduced pressures, annular flow convective condensation heat transfer data over this range can be used to determine the best approach for estimating void fractions under these conditions, as will be shown later in Section 5. The recent database of Cavallini et al. [18,19] will be used for this purpose. They carried out an extensive experimental study on condensation inside a horizontal plain tube of 8.0 mm internal diameter at saturation temperatures ranging from 30 to 60 °C, saturation pressures from 222 to 3150 kPa (reduced pressures from 0.02 to 0.8), mass velocities from 65 to 750 kg/(m^2 s) and vapor qualities from 0.15 to 0.88. The heat transfer data were obtained as quasi-local values as typical of condensing tests using counter-current flow of cooling water with vapor quality changes from inlet to outlet of the test zone (Δx) from about 0.12 to 0.4. From a propagation of errors analysis, they estimated that their heat transfer coefficients were measured to an accuracy of ±5.0% at typical test conditions. Their database of 425 points described in Table 1 is well distributed over their six test fluids as follows: R-22 (106), R-134a (74), R-410A (53), R-125 (73), R-32 (53) and R-236ea (66). These tests represent a significant condensation heat transfer base of high accuracy. Their data categorized as annular flow by the flow pattern map have been used to form the database for developing the new void fraction model in the next section.

5. LMε void fraction method

Void fraction is the foremost parameter in determining two-phase flow pattern transitions, two-phase heat transfer coefficients and two-phase pressure drops. Therefore, it is important to have a method that is both accurate and reliable over the whole range of mass velocities, flow regimes and reduced pressures. At very high reduced pressures, the density of the vapor approaches that of the liquid, at which point the homogeneous void fraction model is applicable, which assumes the vapor and liquid phases travel at the same velocity in the channel. The homogeneous void fraction ε_h is calculated as

$$\varepsilon_h = \left[1 + \left(\frac{1-x}{x}\right)\left(\frac{\rho_V}{\rho_L}\right)\right]^{-1} \tag{1}$$

Of the numerous non-homogeneous void fraction models available, Kattan et al. [3] chose the drift flux model of Rouhani and Axelsson [20] for their flow boiling model over others because drift flux models are more complete in describing the flow and include the effects of mass velocity and surface tension on void fraction, which other methods such as Zivi [16] do not. The Steiner [9] horizontal tube version of the vertical tube expression of Rouhani–Axelsson gives the void fraction ε_{ra} as

$$\varepsilon_{ra} = \frac{x}{\rho_V}\left([1 + 0.12(1-x)]\left[\frac{x}{\rho_V} + \frac{1-x}{\rho_L}\right] + \frac{1.18(1-x)[g\sigma(\rho_L - \rho_V)]^{0.25}}{G\rho_L^{0.5}}\right)^{-1} \tag{2}$$

This method is particularly effective at low to medium pressures but, like other void fraction equations, does not go towards the limit of the homogeneous void fraction as the pressure approaches the critical point. In addition, the Rouhani–Axelsson method was recently introduced into the Kattan–Thome–Favrat flow pattern map for evaporating flows by Thome and El Hajal [21] in order to eliminate the iterative solution involving the liquid height in the former version.

For convective condensation in a turbulent annular film, the convective condensation heat transfer coefficient α_c can be expected to be correlated by the following expression for convective evaporation of Kattan et al. [3], albeit with different empirical constants c and n (also the optimal value of the exponent on the liquid Prandtl number changes from 0.4 to 0.5):

$$\alpha_c = cRe_L^n Pr_L^{0.5}\frac{\lambda_L}{\delta} \tag{3}$$

and assuming $\delta \ll d$, then

$$\delta = \frac{d(1-\varepsilon)}{4} \tag{4}$$

where d is the internal tube diameter, δ is the liquid film thickness for annular flow, ε is the void fraction and the liquid film Reynolds number Re_L is based on the mean velocity of the liquid as

Table 1
Test conditions of Cavallini et al. [18,19]

Fluid	T_{sat} [°C]	p_{sat} [kPa]	G [kg/(m^2 s)]	x_{mean}	Δx	ΔT_{sat} [K]
R-22	40	1550	100	0.21–0.64	0.25–0.4	5.5–8
		1550	200	0.21–0.83	0.2–0.36	5–12
		1480	400	0.26–0.78	0.18–0.39	5–15
		1580	600	0.28–0.84	0.2	7–11
		1490	750	0.23–0.80	0.18–0.28	7–15
R-134a	30	770	400	0.35–0.82	0.23	5–9
	40	1080	65	0.23–0.71	0.23–0.29	3
		1090	100	0.25–0.79	0.15–0.37	2.5–6
		1090	200	0.21–0.78	0.23–0.4	6.5–11
		1040	300	0.25–0.74	0.19–0.31	7–11
		1020	400	0.24–0.77	0.22	6–10
		920	750	0.29–0.80	0.21	7–13
	50	1360	400	0.17–0.75	0.2–0.27	9
	60	1680	400	0.30–0.64	0.2–0.26	9
R-236ea	30	260	200	0.24–0.77	0.22	4–6.7
		246	400	0.28–0.78	0.18	3–6.5
	40	345	100	0.22–0.75	0.2–0.4	3–6
		340	200	0.18–0.77	0.2–0.23	4.4–6.8
		325	400	0.25–0.85	0.17–0.24	4–7.5
		340	600	0.23–0.78	0.16–0.23	3.4–8
	51	482	200	0.26–0.76	0.2–0.31	5–8
		480	400	0.15–0.80	0.17–0.2	3.6–9
R-125	30	1600	200	0.23–0.77	0.27	6–7
		1600	400	0.25–0.77	0.23–0.26	7–9
		1520	750	0.40–0.79	0.18	6–8
	40	1930	100	0.25–0.67	0.22–0.28	3.5
		1930	150	0.25–0.59	0.2–0.4	4–9
		2040	200	0.27–0.78	0.24–0.28	5.5
		2050	400	0.24–0.79	0.27	8–10
		1960	750	0.25–0.79	0.25	8–12
	52	2680	200	0.30–0.65	0.25–0.36	6
		2790	400	0.32–0.82	0.24–0.34	8
		2670	750	0.34–0.75	0.23	6–8
R-32	30	1960	200	0.25–0.65	0.2	5–7
		1930	400	0.30–0.80	0.14–0.22	4–12
		1930	600	0.33–0.81	0.12–0.24	5–14
	40	2500	100	0.37–0.70	0.2–0.39	3.6–7
		2490	200	0.25–0.82	0.18–0.2	5–7
		2480	400	0.25–0.86	0.15–0.2	5–12
		2490	600	0.25–0.80	0.15–0.2	5–13
	50	3140	200	0.25–0.83	0.18–0.2	5–7
		3130	400	0.22–0.86	0.15–0.2	5–12
		3150	600	0.28–0.79	0.15–0.24	6–14
R-410A	28	1770	400	0.40–0.86	0.15	5–7
	40	2380	100	0.37–0.77	0.27–0.4	4.6–7.4

Table 1 (*continued*)

Fluid	T_{sat} [°C]	p_{sat} [kPa]	G [kg/(m^2 s)]	x_{mean}	Δx	ΔT_{sat} [K]
		2420	200	0.21–0.73	0.22–0.39	7–11
		2310	400	0.15–0.88	0.18–0.24	5–12
		2390	750	0.25–0.76	0.21–0.25	10–13
	50	3070	400	0.22–0.83	0.19–0.26	8

$$Re_L = \frac{4G(1-x)\delta}{(1-\varepsilon)\mu_L} = \frac{Gd(1-x)}{\mu_L} \tag{5}$$

which reduces to the second term for annular flows. The convective heat transfer coefficient in annular flow is thus very sensitive to void fraction, such that α_c is proportional to $(1-x)^n/(1-\varepsilon)$, where $\varepsilon > x$ for $x \neq 0$. In fact, for otherwise fixed conditions, the variation of α_c vs. x is only dependent on the variation in ε. Hence, the slopes of experimental curves where α_c is plotted vs. x are in fact determined only by the variation in the void fraction and thus the void fraction model selected controls the slope in α_c vs. x. It is therefore justifiable to utilize accurate annular flow condensation heat transfer data to select the most appropriate void fraction model in the absence of void fraction data at high reduced pressures.

Applying the above equation for α_c to the *annular* flow heat transfer data of Cavallini et al. [18,19] using ε_{ra} for ε and statistically finding the best values for c and n, the convective condensation equation correlates the data reasonably well as shown in Fig. 1 (most data fall within the lines for $\pm 20\%$ error), but the data tend to be segregated by saturation pressure, i.e. from low pressures (R-236ea) up to high pressures (R-410A, R-32 and R-125), with over prediction increasing with pressure. Using instead the maximum possible value of the void fraction, i.e. using ε_h for ε, and statistically finding new values for c and n, the prior trend is reversed with the over prediction increasing with decreasing pressure as shown in Fig. 2. Thus, the effect of pressure is not correctly accounted for by either of the two void fraction expressions. Consequently, it is evident that a void fraction model valid over the entire reduced pressure range is needed. Therefore, several approaches were investigated on how to best interpolate between the values of ε_{ra} and ε_h. A simple logarithmic mean void fraction (LMε) between the values of ε_{ra} and ε_h was found to give the best results (slightly better than a simple arithmetic mean), where the logarithmic mean void fraction ε is defined as

$$\varepsilon = \frac{\varepsilon_h - \varepsilon_{ra}}{\ln\left(\frac{\varepsilon_h}{\varepsilon_{ra}}\right)} \tag{6}$$

The improvement in the prediction is shown in Fig. 3 where the data are no longer segregated by pressure. Hence, this new void fraction expression is valid from low pressures up to those approaching the critical pressure (reduced pressures from 0.02 to 0.8), based on the comparison to the heat transfer data. Fig. 4 shows a comparison of the values of ε_{ra}, ε_h and ε (that is LMε) for R-410A at saturation conditions of 40 °C and 2410 kPa ($p_r = 0.5$). The most significant differences are at low vapor qualities. Still, the seemingly insignificant differences at high vapor qualities actually have a significant

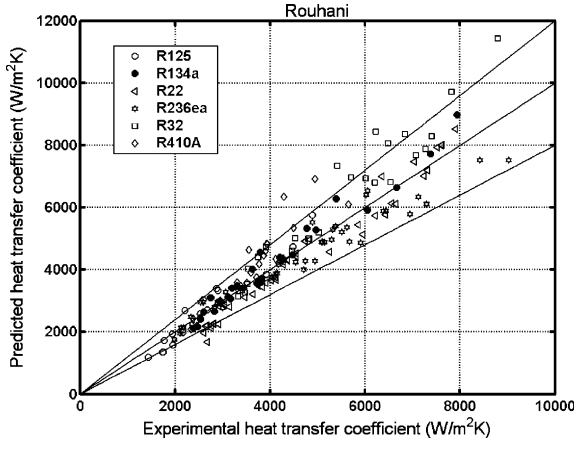

Fig. 1. Comparison of experimental to predicted values using ε_{ra} for ($c = 0.0099$, $n = 0.636$).

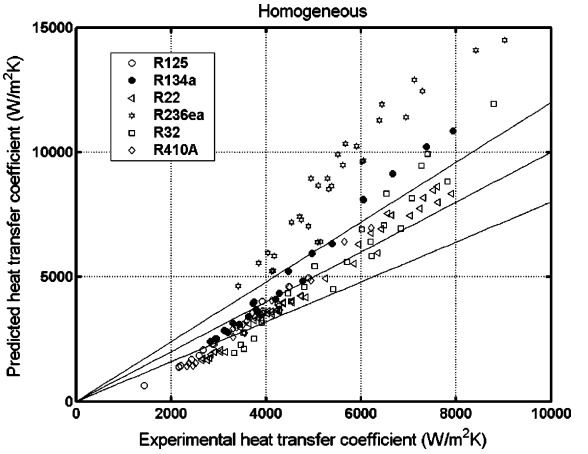

Fig. 2. Comparison of experimental to predicted values using ε_h for ε ($c = 0.0000785$, $n = 1.115$).

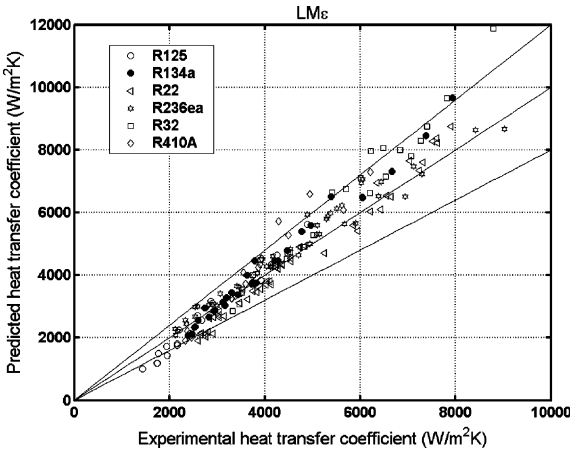

Fig. 3. Comparison of experimental to predicted values using LMε for ε ($c = 0.0039$, $n = 0.734$).

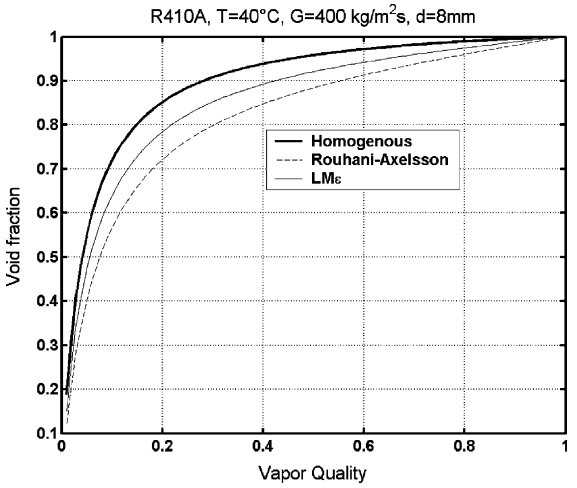

Fig. 4. Comparison of void fraction methods for R-410A.

effect on α_c, e.g. a decrease in void fraction from 0.99 to 0.98 doubles the film thickness δ in Eq. (3).

6. New version of flow pattern map for condensation

Fig. 5 from Collier and Thome [22] depicts some of the typical flow regimes observed during evaporation and condensation inside a horizontal tube, including some cross-sectional views of the flow structure. The flow patterns observed are bubbly flow, plug flow, slug flow, stratified-wavy flow, annular flow and annular flow with partial dryout (in evaporation). Presently, flow patterns are classified as follows: *fully-stratified* flow (**S**), *stratified-wavy* flow (**SW**), *intermittent* flow (**I**), *annular* flow (**A**), *mist* flow (**MF**) and *bubbly* flow (**B**). Intermittent flow refers to both the *plug* and *slug* flow regimes (it is essentially a stratified-wavy flow pattern with large amplitude waves that wash the top of the tube). Also, stratified-wavy flow is often referred to in the literature as simply *wavy* flow. For a detailed definition of the flow patterns used here, refer to those in Collier and Thome [22].

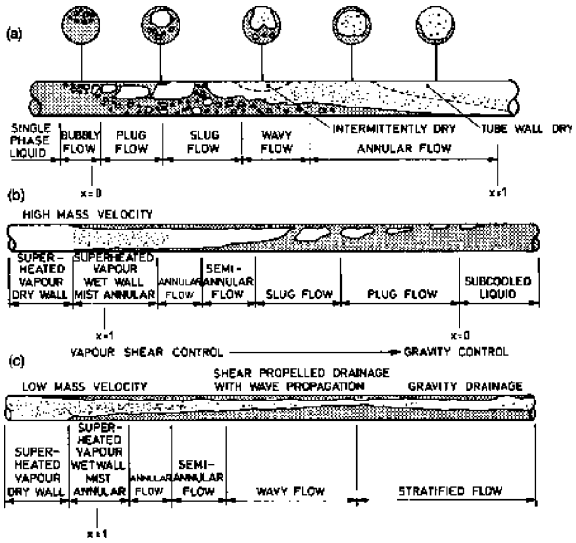

Fig. 5. Two-phase flow patterns in horizontal tubes from Collier and Thome [22]: (a) evaporation, (b) condensation with high liquid loading, (c) condensation with low liquid loading.

The flow pattern map modified here is that of Kattan et al. [1] for evaporation and adiabatic flows in small diameter horizontal tubes. Their map is a modification of the Steiner [9] map, which in turn is a modification of the original Taitel and Dukler [6] map. Zürcher et al. [23] have proposed an updated version of this map with two adjustments based on new flow pattern observations for ammonia taken at mass velocities down to about 16 kg/(m^2 s). More recently, Thome and El Hajal [21] have simplified implementation of the map by bringing the Rouhani–Axelsson void fraction equation into the method to eliminate its iterative solution scheme. It is this last version that is the starting point here for the condensation flow map.

The flow pattern map for evaporation is shown in Fig. 6 for R-134a in an 8.0 mm tube at a saturation temperature of 40 °C. The transition boundary between annular flow (A) and stratified-wavy (SW) flow at high vapor quality represents the onset of dryout of the annular film and is thus a function of heat flux. For condensation, saturated vapor enters a condenser tube and forms either (i) a thin liquid film around the perimeter of the tube as an annular flow or (ii) a liquid layer in the bottom of the tube and a gravity-controlled condensing film around the upper perimeter as a stratified or stra-

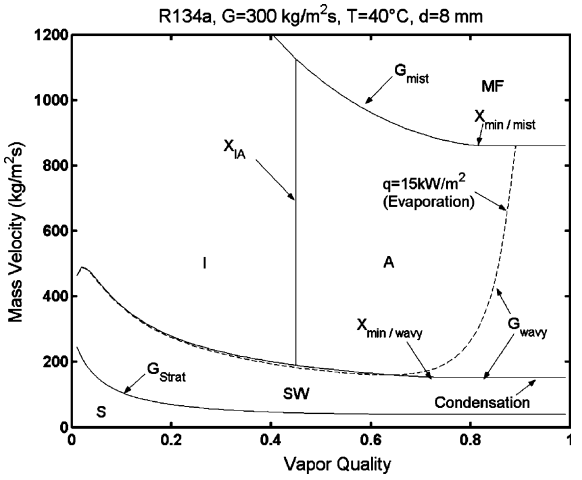

Fig. 6. Kattan–Thome–Favrat flow pattern map illustrating G_{wavy} transition boundaries for evaporation and condensation.

tified-wavy flow. Hence, dryout does not occur for condensation. Therefore, the transition curve labeled G_{wavy} can be supposed to reach its minimum value and then continue on horizontally to the vapor quality of 1.0, as shown in Fig. 6. This means that a saturated vapor enters at $x = 1.0$ and goes directly into either the annular flow regime or the stratified-wavy flow regime, depending on whether G is greater or less that G_{wavy}. The other boundaries remain the same, assuming the gravity-controlled condensing film around the upper perimeter does not affect them. The bubbly flow regime occurs at mass velocities higher than those shown on the present map and this regime is also beyond the range of our current database. In a mist flow, it can be envisioned that the layer of condensate will be sheared from the wall and that a new condensate layer will begin to grow again in its place.

Fig. 7 defines the geometrical dimensions of a stratified flow, where P_{L} is the stratified perimeter around the bottom of the tube, P_{V} is the non-stratified perimeter around the top of the tube, h_{L} is the height of the stratified liquid, P_{i} is the length of the interface, and A_{L} and A_{V} are the corresponding cross-sectional areas occupied by the liquid and vapor. Four of these dimensions are normalized using the tube internal diameter d to obtain four dimensionless variables:

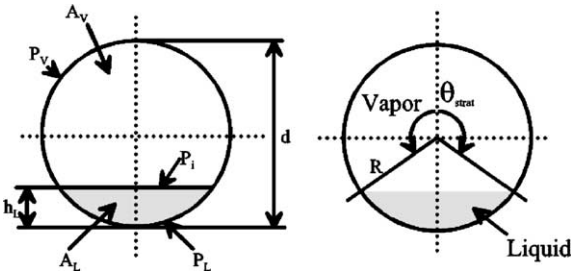

Fig. 7. Geometrical parameters for two-phase flow in a circular tube.

$$h_{\text{Ld}} = \frac{h_{\text{L}}}{d}, \quad P_{\text{id}} = \frac{P_{\text{i}}}{d}, \quad A_{\text{Ld}} = \frac{A_{\text{L}}}{d^2}, \quad A_{\text{Vd}} = \frac{A_{\text{V}}}{d^2} \tag{7}$$

Rather than using the Rouhani–Axelsson void fraction equation to obtain ε as in Thome and El Hajal [21], the new LMε void fraction equation is used for ε in order to extend application of the flow pattern map to high reduced pressures. Then, from the cross-sectional area of the tube A, the values of A_{L}, A_{V}, A_{Ld} and A_{Vd} are directly determinable as

$$A_{\text{L}} = A(1-\varepsilon) \tag{8}$$

$$A_{\text{V}} = A\varepsilon \tag{9}$$

The area A_{L} here ignores any liquid formed by film condensation on the upper perimeter of the tube. The stratified angle θ_{strat} in Fig. 7 remains the only parameter which must be solved for in an iterative manner from the following geometrically defined equation:

$$A_{\text{Ld}} = \tfrac{1}{8}[(2\pi - \theta_{\text{strat}}) - \sin(2\pi - \theta_{\text{strat}})] \tag{10}$$

(*Note:* A non-iterative expression equivalent to Eq. (10) is given as Eq. (19) in Part 2.) The dimensionless liquid height can then be determined from the geometric expression:

$$h_{\text{Ld}} = 0.5\left(1 - \cos\left(\frac{2\pi - \theta_{\text{strat}}}{2}\right)\right) \tag{11}$$

The geometric expression for P_{id} in terms of θ_{strat} is

$$P_{\text{id}} = \sin\left(\frac{2\pi - \theta_{\text{strat}}}{2}\right) \tag{12}$$

The transition curve from stratified-wavy flow to intermittent and annular flow for *evaporation* is determined using the updated expression of Zürcher et al. [23] for G_{wavy}, where G_{wavy} is in kg/(m^2 s):

$$G_{\text{wavy}} = \left\{ \frac{16A_{\text{Vd}}^3 g d \rho_{\text{L}} \rho_{\text{V}}}{x^2\pi^2(1-(2h_{\text{Ld}}-1)^2)^{0.5}} \left[\frac{\pi^2}{25h_{\text{Ld}}^2}(1-x)^{-F_1(q)} \times \left(\frac{We}{Fr}\right)_{\text{L}}^{-F_2(q)} + 1 \right] \right\}^{0.5} + 50 - 75\mathrm{e}^{-(x^2-0.97)^2/x(1-x)} \tag{13}$$

The non-dimensional empirical exponents accounting for the effect of heat flux on dryout during evaporation are $F_1(q)$ and $F_2(q)$:

$$F_1(q) = 646.0\left(\frac{q}{q_{\text{crit}}}\right)^2 + 64.8\left(\frac{q}{q_{\text{crit}}}\right) \tag{14}$$

$$F_2(q) = 18.8\left(\frac{q}{q_{\text{crit}}}\right) + 1.023 \tag{15}$$

where the critical heat flux q_{crit} was used to normalize the local heat flux. The heat flux effect on dryout is not required for condensation and hence $q = 0$. Thus, the values of F_1 and F_2 become 0 and 1.023, respectively, for condensation and G_{wavy} for *condensation* becomes

$$G_{wavy} = \left\{ \frac{16A_{Vd}^3 g d \rho_L \rho_V}{x^2\pi^2(1-(2h_{Ld}-1)^2)^{0.5}} \left[\frac{\pi^2}{25h_{Ld}^2} \times \left(\frac{We}{Fr} \right)_L^{-1.023} + 1 \right] \right\}^{0.5} + 50 - 75e^{-(x^2-0.97)^2/x(1-x)} \tag{16}$$

This expression is solved for the minimum value of the transition to find $(G_{wavy})_{min}$ and the value of x at which this occurs is designated as x_{min}. Then, for all $x > x_{min}$, $G_{wavy} = (G_{wavy})_{min}$ as shown in Fig. 6.

Similarly, the transition curve from stratified-wavy flow to fully stratified flow is determined using the other updated expression of Zürcher et al. [23] for G_{strat}, where G_{strat} is in kg/(m^2 s):

$$G_{strat} = \left\{ \frac{(226.3)^2 A_{Ld} A_{Vd}^2 \rho_V (\rho_L - \rho_V) \mu_L g}{x^2(1-x)\pi^3} \right\}^{1/3} + 20x \tag{17}$$

The transition between intermittent flow and annular flow is a vertical line given by x_{IA}, which is determined by setting the Martinelli parameter X_{tt} equal to 0.34, as

$$x_{IA} = \left\{ \left[0.2914 \left(\frac{\rho_V}{\rho_L} \right)^{-1/1.75} \left(\frac{\mu_L}{\mu_V} \right)^{-1/7} \right] + 1 \right\}^{-1} \tag{18}$$

This transition has a lower bound where it intersects the transition curve of G_{wavy} as shown in Fig. 6 and has an upper bound where it intersects the transition curve of G_{mist}. The transition curve from annular and intermittent flow to mist flow gives G_{mist} in kg/(m^2 s) as

$$G_{mist} = \left\{ \frac{7680 A_{Vd}^2 g d \rho_L \rho_V}{x^2\pi^2\xi} \left(\frac{Fr}{We} \right)_L \right\}^{0.5} \tag{19}$$

In the above equation, the ratio of the liquid Weber number We_L to the liquid Froude number Fr_L is

$$\left(\frac{We}{Fr} \right)_L = \frac{g d^2 \rho_L}{\sigma} \tag{20}$$

and the factor ξ is

$$\xi = \left[1.138 + 2\log\left(\frac{\pi}{1.5A_{Ld}} \right) \right]^{-2} \tag{21}$$

This expression is first evaluated at all values of x to find the minimum value of G_{mist}, which is set to $(G_{mist})_{min}$ at x_{min}, and then $G_{mist} = (G_{mist})_{min}$ for all values of x for $x > x_{min}$ as observable in Fig. 6. Finally, the last transition is that to bubbly flow G_{bubbly}, which is in kg/(m^2 s):

$$G_{bubbly} = \left\{ \frac{256 A_{Vd} A_{Ld}^2 d^{1.25} \rho_L (\rho_L - \rho_V) g}{0.3164(1-x)^{1.75}\pi^2 P_{id} \mu_L^{0.25}} \right\}^{1/1.75} \tag{22}$$

Bubbly flow occurs at very high mass velocities that are above the range shown in Fig. 6.

The parameters required to evaluate the condensation flow pattern transitions are: tube internal diameter (d), vapor quality (x), total mass velocity of the liquid and vapor (G), liquid density (ρ_L), vapor density (ρ_V), liquid dynamic viscosity (μ_L), vapor dynamic viscosity (μ_V) and surface tension (σ). The local flow pattern is determined by the following procedure:

1. Input: values of d, G and x ($0 < x < 1$) and physical properties;
2. Evaluate Eqs. (1), (2) and (6) to find ε_h, ε_{ra} and ε;
3. Evaluate Eqs. (8) and (9) to find A_L and A_V and then use Eq. (7) to obtain A_{Ld} and A_{Vd};
4. Solve Eq. (10) iteratively, or use Eq. (19) in Part 2, to find θ_{strat};
5. Evaluate Eqs. (11) and (12) to obtain h_{Ld} and P_{id};
6. Evaluate Eq. (16) over a range of x to find G_{wavy} and x_{min};
7. Evaluate Eqs. (17) and (18) to find G_{strat} and x_{IA};
8. Evaluate Eqs. (20) and (21) to get $(We/Fr)_L$ and ξ and then find G_{mist} and G_{bubbly} from Eqs. (19) and (22);
9. Compare the values obtained to those input for x and G to identify the particular flow pattern.

For the flow pattern transitions during the thermal design of a condenser (and in our comparisons to data), the design value of G is used to evaluate ε_{ra}. To construct a flow pattern map for visualization purposes, it is sufficient to assume a fixed value G in the general range of interest. The choice of the value of G affects the void fraction calculation (see Section 8 for an illustration of this point) but is not very significant for the principal transition curves of interest here (G_{strat} and G_{wavy}) and has no impact on x_{IA}.

To identify the flow pattern at a particular value of vapor quality x, the following logic is applied:

Annular flow exists if $G > G_{wavy}$, $G < G_{mist}$ and $x > x_{IA}$;
Intermittent flow exists if $G > G_{wavy}$, $G < G_{mist}$ or $G < G_{bubbly}$ and $x < x_{IA}$;
Stratified-wavy flow exists if $G_{strat} < G < G_{wavy}$;
Fully stratified flows exists if $G < G_{strat}$;
Mist flow exists if $G > G_{mist}$.

7. Comparison to other transition criteria

Before proceeding with these comparisons, it should be pointed out that flow patterns for stratified-wavy flow

obtained in a tubular sight glass at the end of a condenser tube will tend to look like an annular or an intermittent flow because of the Nusselt film condensation process on the perimeter of the tube above the waves. Hence, methods based on flow pattern observations in sight glasses located at the ends of condenser heat transfer test sections will tend to result in lower transition boundaries between these regimes. It is preferable to deal with Nusselt film condensation as part of the heat transfer model rather than in the flow pattern transition so as to be able to distinguish between the two types of heat transfer mechanisms occurring locally around the perimeter of the tube, i.e. either forced convection to an axially flowing film or gravity-driven condensation as a falling film. Also, to minimize confusion for the comparisons on the following graphs, our flow pattern regions are indicated by their letter symbols (**S**, **SW**, **A**, **I** and **MF**) while those of the other transition criteria are indicated by the complete name of each regime.

7.1. Comparison between old and new LMε maps

The effect of using the LMε void fraction expression in place of the Rouhani–Axelsson void fraction equation is shown in Fig. 8 for R-134a at 40 °C ($p_{sat} = 1017$ kPa and $p_r = 0.25$) in an 8 mm tube, setting $G = 300$ kg/(m^2 s) for evaluation of the void fractions for illustration purposes. This is near the maximum pressure in the underlying database of flow pattern observations in the prior evaporation version of this map. As can be seen, there is no effect on x_{IA} and an extremely minor effect on G_{strat} when replacing ε_{ra} with LMε. The effect on G_{wavy} is to raise that transition curve by about 20 kg/(m^2 s) over most of the vapor quality range, which is not significant considering the transition zone around these curves on the order of ±50 kg/(m^2 s) when passing from one stable flow pattern to another. The difference between the two G_{mist} curves is more significant but the location of this curve is not critical to the condensation heat transfer model since the annular flow heat transfer model is found to predict mist flow heat transfer data reasonably well in Part 2.

7.2. Breber, Palen and Taborek

A flow pattern map for condensation was proposed by Breber et al. [10] using a broad database (unfortunately their flow pattern database is no longer available according to Palen). Rather than utilizing the flow pattern definitions used here, they classified flow regimes as *wavy + stratified*, *annular + mist-annular* (annular flow with entrained mist), *intermittent* (*slug + plug*) and *bubbly* and also include some transition regions in between these regimes. Hence, it is not possible to make a quantitative comparison between these two approaches. Transforming their map of dimensionless gas velocity vs. Martinelli parameter to our format of G vs. x, Fig. 9 illustrates a comparison for R-12 (a fluid in their database) at 40 °C in an 8 mm tube using $G = 300$ kg/(m^2 s) for calculating our map. (To visualize their flow pattern regions on this *busy* graph, imagine zones bounded by the dashed lines.) Comparing our G_{wavy} transition to their transition region between wavy + stratified and annular + mist-annular, the agreement is quite good considering that there should be a transition zone of about ±50 kg/(m^2 s) surrounding the G_{wavy} curve. Also, their zone of wavy + stratified falls within our zones of stratified-wavy and stratified flows, again showing qualitative agreement between the two approaches. Their slug + plug regime is equivalent to our intermittent

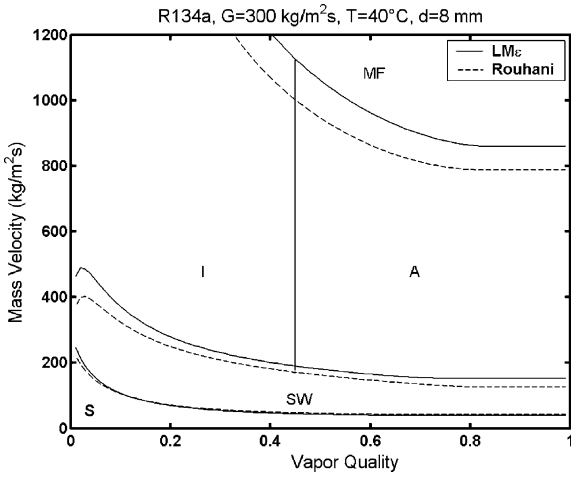

Fig. 8. Flow pattern map comparison for R-134 at 40 °C in an 8 mm tube.

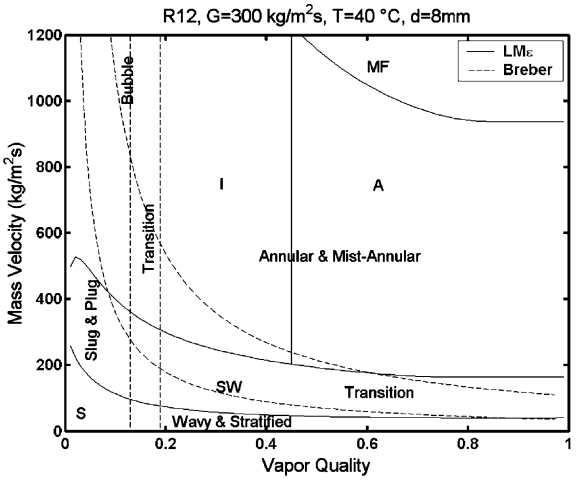

Fig. 9. Comparison to Breber et al. [10] map for R-12 at 40 °C in an 8 mm tube.

regime, and it is seen that their zone falls within our intermittent flow zone but their transition zone is to the left of our x_{IA} transition line (which probably means that their observations under these circumstances are our intermittent flows, which we define as large amplitude intermittent waves that wash the top of the tube and leave behind liquid films). They also have a bubble regime at high mass velocities, which overlaps with our bubble flow regime (at values of G greater than those shown). Thus, the qualitative agreement between these two maps is quite reasonable.

7.3. Tandon, Varma and Gupta

In their map, Tandon et al. [11] defined flow regimes as *wavy*, *plug*, *slug*, *annular + semi-annular* and *spray*. Semi-annular apparently refers to annular flows in which the liquid film is much thicker at the bottom than the top of the tube; spray flow apparently refers to an annular flow with significant liquid entrainment in the central vapor core. Converting their map to our format of G vs. x, Fig. 10 shows a comparison for R-12 (a fluid in their database) at 40 °C in an 8 mm tube using $G = 300$ kg/(m^2 s) for calculating our map. Their transition curve between wavy flow and annular + semi-annular is similar to our curve for G_{wavy}, although the discrepancy becomes large at high vapor qualities. Furthermore, their slug flow regime falls within our intermittent flow regime as it should. Instead, their plug regime falls within our stratified regime at very low vapor qualities, where there may not be enough vapor to form a continuous vapor phase for a stratified flow (but the only plug flow data shown in their paper are located in their slug flow region). Their annular + semi−annular regime is apparently analogous to our annular and intermittent regimes (with the exclusion of slug flows as a separate regime in their map) and these two zones overlap reasonably well. Their spray flow regime would be classified as an annular flow in our map and hence these two zones also more or less coincide. Hence, taking into account the different flow regime definitions, the qualitative agreement between these two maps is still quite reasonable.

7.4. Sardesai, Owen and Pulling

Sardesai et al. [13] have applied the recommendations in the German *VDI HeatAtlas* for transition between *non-stratified* flow and *stratified* flow with an intermediate transition zone in developing their condensation prediction method. Fig. 11 shows these transitions represented on our map for R-12 at 40 °C in an 8 mm tube. Their lower transition is from wavy + stratified flow to the transition zone between wavy to annular flow while their upper transition is to stable annular flow. Hence, our stratified flows and some of our stratified-wavy flows fall correctly below their lower transition curve and our annular flow transition (G_{wavy}) correctly falls just above their annular flow transition curve. Our stratified-wavy flows above their lower transition curve fall within their transition zone. Hence, their flow pattern zones fall correctly within ours.

7.5. Cavallini, Censi, Del Col, Doretti, Longo and Rossetto

The flow pattern map proposed by Cavallini et al. [5] is a composite of selected flow transition criteria proposed by others formulated into a single map, where some transition boundaries were adapted to the corre-

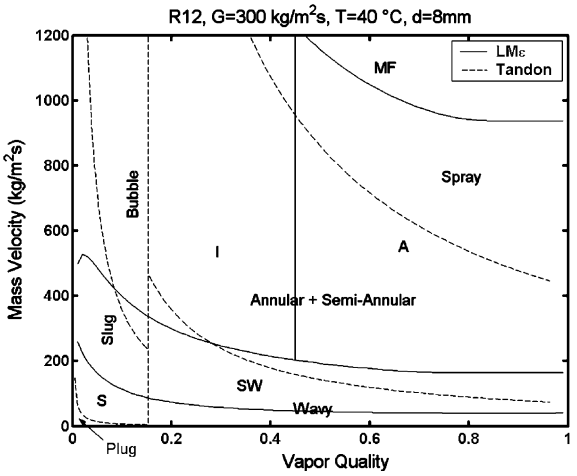

Fig. 10. Comparison to Tandon et al. [11] map for R-12 at 40 °C in 8 mm tube.

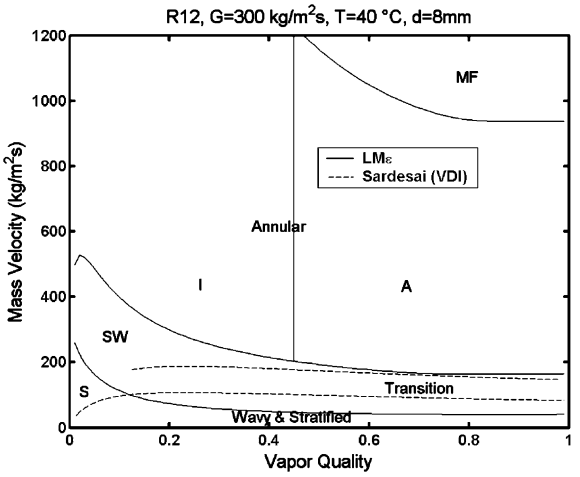

Fig. 11. Comparison to Sardesai et al. [13] transitions for R-12 at 40 °C in an 8 mm tube.

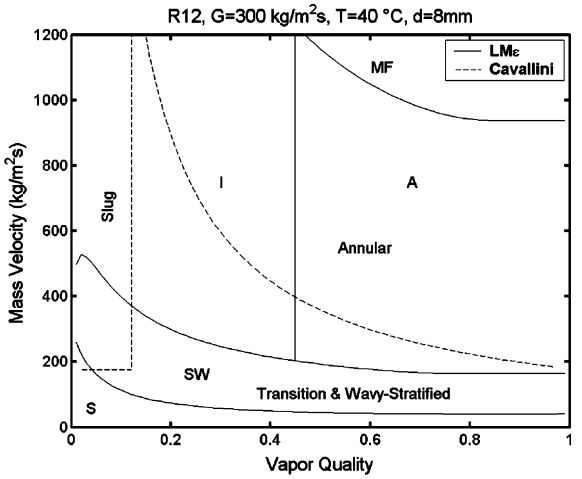

Fig. 12. Comparison to Cavallini el al. [5] map for R-12 at 40 °C in an 8 mm tube.

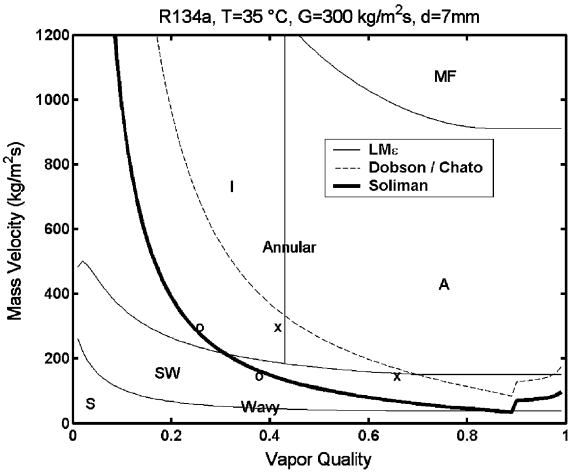

Fig. 13. Comparison to Dobson and Chato [15] and Soliman [24] transitions for R-134a at 35 °C in a 7 mm tube.

sponding transitions noted in the trends of their heat transfer data. Fig. 12 depicts their map converted to our G vs. x format and compared with our map for R-12 at 40 °C in an 8 mm tube. In their map, they classify flows as *annular*, *transition + stratified-wavy* and *slug* flows. As can be seen, their annular flow region coincides with our annular flow zone and their slug flow region for the most part correctly falls within our intermittent flow zone. The definition of their transition + stratified-wavy zone is not well defined and this may refer to our intermittent and stratified-wavy zones. They, like most others for condensation, completely ignore the fully stratified (S) zone that is included in our map.

7.6. Dobson–Chato, Soliman and Shao-Granryd

Dobson and Chato [15] adopted a wavy flow transition criterion proposed by Soliman [24] for their condensation heat transfer model, but increased the transition value of Soliman's Froude number from 7 to 20 to better represent their heat transfer data, which were classified as *wavy* and *annular* flows. Similarly, Shao and Granryd [4] also found that the best value for Fr to be from 15 to 20 based on their data. Fig. 13 depicts a comparison of both the Dobson–Chato and the Soliman transition curves to G_{wavy} for R-134a at 35 °C in a 7 mm tube, conditions which they tested (a curve for $Fr = 15$ is not shown but would lie in between the curves for 7 and 20). Both these transition curves intersect the G_{wavy} curve but do not match its predictions at high and low vapor qualities. The "jump" occurring in their curves at high vapor qualities is caused by the liquid Reynolds number passing through the transition from turbulent to laminar flow at $Re_L = 1250$ in their method. Also plotted are the four flow pattern observations presented by Dobson and Chato for transitions from *stable wavy* flow to the mixed regime of *wavy* & *annular* flow (o) and then from this *wavy* & *annular* flow to *stable annular* flow (x). The first two transitions conform reasonably well to our transition from wavy to intermittent flow (intermittent flow could appear as a cycling between wavy and annular flow) and one of the other two observations is near our transition from wavy to annular flow at a vapor quality of 0.66. The last observation at $x = 0.41$ is near our intermittent to annular flow transition x_{IA}, which could presumably define what they saw as well. Hence, all four of these observations seem to fit our map. Our transition equations were evaluated setting $G = 300$ kg/(m^2 s) while two of their data are at 150 kg/(m^2 s), but this has little effect on the location of these particular curves.

Shao and Granryd [4] presented six flow pattern observations reported to be near transition for R-134a, R-22 and R-502 for a 6 mm bore sight glass, plotted here in Fig. 14. In the top graph, their two R-134a annular (A) and wavy (W) observations are correctly categorized by our map. In the middle graph, their R-22 annular (A) observation is correctly identified while their wavy (W) observation is just above the respective transition curve by about 3 kg/(m^2 s), which again confirms the validity of the map. In the bottom graph, their R-502 wavy (W) observation is correctly identified while their other wavy (W) observation is about 25 kg/(m^2 s) above the respective transition curve, which is within the $\pm$50 kg/(m^2 s) transition zone from one stable flow regime to another that surrounds all the transition curves. Hence, five of the six observations for three different refrigerants can be considered as correctly identified (83%) while the sixth one is in the vicinity of the transition curve.

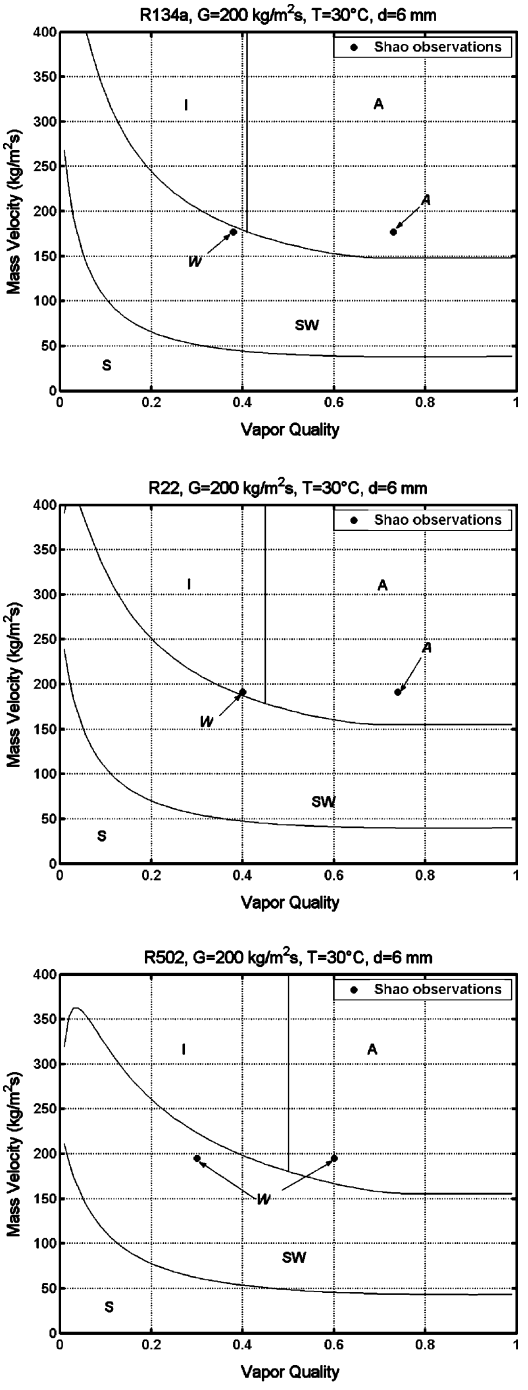

Fig. 14. Flow pattern observations of Shao and Granryd [4] compared to map.

In summary, the subjective nature of classifying flow pattern observations from one observer to another, the difference in opinion on flow pattern definitions, and even disagreement about which classifications to use, means that a quantitative comparison between competing methods is not always realistic. Even so, numerous similarities and overlaps between flow regime zones and flow transition boundaries are found in the above comparisons, good agreement between the map and some recent flow pattern observations has been shown, and these document that it is justifiable to apply a broad interpretation of the general applicability of the new condensation flow pattern map based on the logarithmic mean void fraction (LMε).

8. Effects of variables on flow pattern transitions

To illustrate the effect of important variables (mass velocity, reduced pressure, tube diameter, fluid properties) on the new flow pattern map for condensation, four comparisons have been prepared below to show their predicted effects on flow pattern transition boundaries.

8.1. Mass velocity

All the flow regime transition equations are dependent on the mass velocity G that is input into the Rouhani–Axelsson void fraction equation, except for the vertical transition line x_{IA}. Normally, the design value of G is used for evaluating the map at the flow rate being considered in the condenser. On the other hand, it is also convenient to generate a flow pattern map to see where flow regime transitions are and thus choose design variables to force the design into specific regimes. To correctly illustrate a complete flow pattern map, ideally the mass velocity should be increased in small steps and the various transition points (G, x) then determined. From a practical point of view (for visualization of the map but not for its application), it is more convenient to ignore the effect of G on ε by choosing a fixed value of G in the general range of interest to calculate the transition points. In Fig. 15, a comparison is made for R-134a at a saturation temperature of 40 °C in an 8.0 mm tube where the transitions have been calculated using three different fixed values of G: 25, 300 and 1000 kg/(m^2 s). As can be seen, using a value of 300 or 1000 has little significant difference on the transitions but using $G = 25$ significantly affects the curves of G_{wavy} and G_{mist} compared to $G = 300$ (but these transitions are a long way away for someone interested in what is happening near $G = 25$). Hence, it is best to choose an intermediate value of 300 kg/(m^2 s) since it has minimal effect on G_{strat} and it is a mean value for G_{wavy} curves.

8.2. Reduced pressure

Flow pattern transitions for R-134a at reduced pressures of 0.072 (0 °C), 0.25 (40 °C) and 0.80 (90 °C) are shown in Fig. 16. The effect on G_{strat} is shown to not

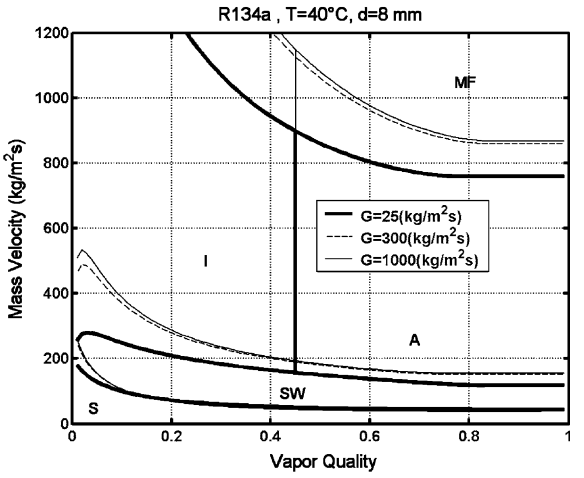

Fig. 15. R-134a flow pattern maps at 40 °C for an 8.0 mm tube evaluated using three values of G (kg/m^2 s).

be very significant. The effect on G_{wavy} is evident, especially at low vapor qualities, while at high vapor qualities the transition boundary tends to rise with increasing reduced pressure. The x_{IA} boundary moves noticeably to high vapor qualities with increasing reduced pressure from about 0.28–0.66. The effect on G_{mist} is the largest, increasing from 0 to 40 °C and then decreasing again at 90 °C. Interestingly, as the pressure approaches the critical pressure, the G_{mist} curve continues towards smaller mass velocities, which, in essence, means that the map predicts that the mist flow zone dominates over nearly all mass velocities at high reduced pressures and that the entrained droplet and vapor velocities become similar in value, which is the natural limit as $p_{sat} \rightarrow p_{crit}$.

8.3. Tube diameter

In Fig. 17, a comparison is made for tubes of 3, 8 and 22 mm where the transitions have been calculated using $G = 300$ kg/(m^2 s). There are no effects on G_{strat} and x_{IA}. For G_{wavy} the transition goes to lower mass velocity values as the diameter decreases. The effect on G_{mist} is very large where the transition mass velocity increases as the diameter decreases. These latter two trends are similar to those observed by Dobson and Chato [15].

8.4. Comparison of fluids

In Fig. 18, transitions for R-134a, R-22 and R-410A are compared at a saturation temperature of 40 °C for an 8.0 mm tube and setting $G = 300$ kg/(m^2 s). The reduced pressures for these three fluids at 40 °C are 0.25, 0.30 and 0.50, respectively. For the transitions of principal interest to condensation heat transfer, i.e. G_{strat} and G_{wavy}, there are only minor differences except at very low vapor qualities. The transitions from intermittent to annular flow are at vapor qualities of 0.45, 0.49 and 0.55. The effect on G_{mist} is the most significant where R-410A has the lowest transition threshold and R-22 the highest.

9. Range of application

Based on the database of Part I, that in Part II, and those for evaporation of Thome and coworkers, the current map is expected to be reliable and accurate over the following range of parameters: $16 < G < 1532$ kg/(m^2 s); $3.14 < d < 21.4$ mm; $0.02 < p_r < 0.8$; $76 < (We/Fr)_L < 884$. So far, it has been utilized with the following twenty fluids: ammonia, R-11, R-12, R-22,

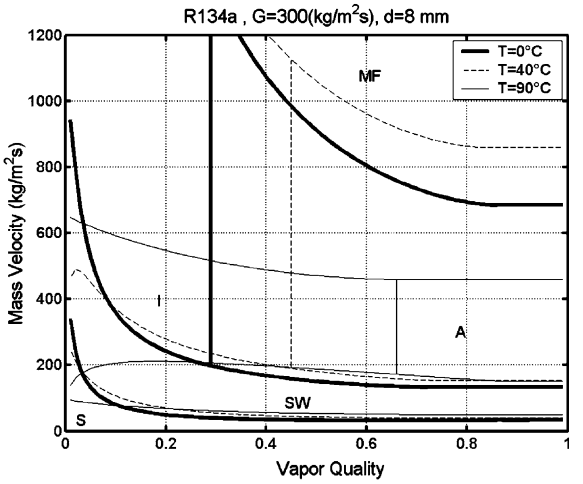

Fig. 16. R-134a flow pattern maps for an 8.0 mm tube evaluated at three reduced pressures.

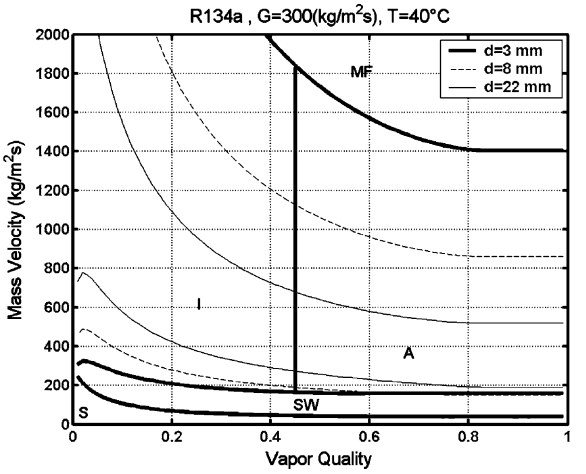

Fig. 17. Flow pattern transitions for 3, 8 and 22 mm tubes for R-134a at 40 °C.

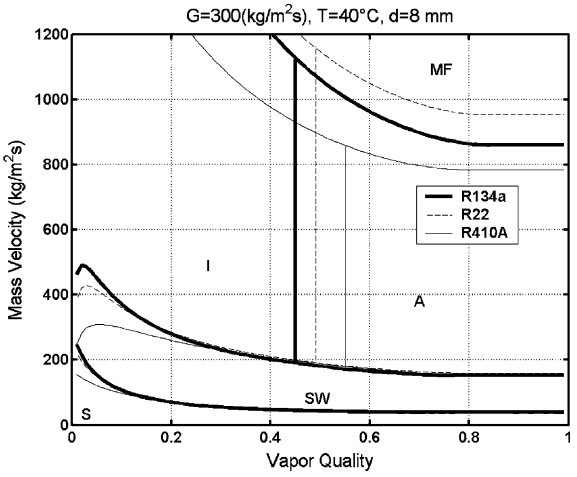

Fig. 18. Flow pattern transitions for R-134a, R-22 and R-410A in an 8 mm tube at 40 °C.

R-32, R-113, R-123, R-125, R-134a, R-236ea, R-32/R-125 near azeotrope, R-402A, R-404A, R-407C, R-410A, R-502, propane, *n*-butane, iso-butane and propylene.

10. Conclusions

A new flow pattern map for condensation in horizontal plain tubes has been proposed. This map is an extension of the Kattan et al. [1] map for *evaporating and adiabatic flows* to *condensation* and to *high reduced* pressures. The new flow pattern map incorporates a newly defined logarithmic mean void fraction (LMε) method for calculation of vapor void fractions spanning the entire range from low pressures up to pressures near the critical point. In the absence of void fraction data at high reduced pressures, the new LMε method was indirectly validated using the convective condensation model for annular flow for reduced pressures from 0.02 up to 0.8. The new map has also been successfully compared to some recent flow pattern observations (quantitative agreement) and to other flow pattern transition methods (qualitative agreement). In Part 2, this map is shown to be very successful for incorporating our new condensation heat transfer model, attaining very high accuracies in comparisons to a database composed of test data from nine independent laboratories.

Acknowledgement

A. Cavallini participated in this project as an ER-COFTAC Scientific Visitor to the Laboratory of Heat and Mass Transfer in Lausanne.

References

[1] N. Kattan, J.R. Thome, D. Favrat, Flow boiling in horizontal tubes: Part 1—Development of a diabatic two-phase flow pattern map, J. Heat Transfer 120 (1998) 140–147.
[2] N. Kattan, J.R. Thome, D. Favrat, Flow boiling in horizontal tubes: Part 2—New heat transfer data for five refrigerants, J. Heat Transfer 120 (1998) 148–155.
[3] N. Kattan, J.R. Thome, D. Favrat, Flow boiling in horizontal tubes: Part 3—Development of a new heat transfer model based on flow pattern, J. Heat Transfer 120 (1998) 156–165.
[4] D.W. Shao, E.G. Granryd, Flow pattern, heat transfer and pressure drop in flow condensation, Part 1: Pure and azeotropic refrigerants, Int. J. HVAC&R Res. 6 (2) (2000) 175–195.
[5] A. Cavallini, G. Censi, D. Del Col, L. Doretti, G.A. Longo, L. Rossetto, Intube condensation of halogenated refrigerants, ASHRAE Trans. 108 (1) (2002), Paper 4507.
[6] Y. Taitel, A.E. Dukler, A model for predicting flow regime transitions in horizontal and near horizontal gas–liquid flow, AIChE J. 22 (2) (1976) 43–55.
[7] O. Baker, Design of pipelines for simultaneous flow of oil and gas, Oil Gas J. 53 (1954) 185–195.
[8] K. Hashizume, Flow pattern and void fraction of refrigerant two-phase flow in a horizontal pipe, Bull. JSME 26 (219) (1983) 1597–1602.
[9] D. Steiner, Heat transfer to boiling saturated liquids, in: VDI-Wär meatlas (VDI Heat Atlas), Chapter Hbb, VDI-Gessellschaft Verfahrenstechnik und Chemieingenieurwesen (GCV), Düsseldorf, 1993 (Translator: J.W. Fullarton).
[10] G. Breber, J.W. Palen, J. Taborek, Prediction of horizontal tube-side condensation of pure components using flow regime criteria, J. Heat Transfer 102 (1980) 471–476.
[11] T.N. Tandon, H.K. Varma, C.P. Gupta, A new flow regime map for condensation inside horizontal tubes, J. Heat Transfer 104 (1982) 763–768.
[12] W.W. Ackers, H.F. Rosson, Condensation inside a horizontal tube, Chem. Eng. Prog. Symp. Series 56 (1960) 145–149.
[13] R.G. Sardesai, R.G. Owen, D.J. Pulling, Flow regimes for condensation of a vapour inside a horizontal tube, Chem. Eng. Sci. 36 (1981) 1173–1180.
[14] M.M. Shah, A general correlation for heat transfer during film condensation inside pipes, Int. J. Heat Mass Transfer 22 (1979) 547–556.
[15] M.K. Dobson, J.C. Chato, Condensation in smooth horizontal tubes, J. Heat Transfer 120 (1998) 193–213.
[16] S.M. Zivi, Estimation of steady state void fraction by means of minimum entropy production, J. Heat Transfer 86 (1964) 247–252.
[17] D. Chisholm, An equation for velocity ratio in two-phase flow, NEL report, Scotland, 1972.
[18] A. Cavallini, D. Del Col, G.A. Longo, L. Rossetto, Condensation heat transfer with refrigerants, in: Proceedings of Two-Phase Flow Modelling and Experimentation Conference, ETS, Pisa, vol. 1, 1999, pp. 71–88.
[19] A. Cavallini, D. Del Col, G.A. Longo, L. Rossetto, Experimental investigation on condensation heat transfer and pressure drop of new HFC refrigerants (R134a, R125,

R32, R410A, R236ea) in a horizontal tube, Int. J. Refrig. 24 (2001) 73–87.

[20] Z. Rouhani, E. Axelsson, Calculation of void volume fraction in the subcooled and quality boiling regions, Int. J. Heat Mass Transfer 13 (1970) 383–393.

[21] J.R. Thome, J. El Hajal, Two-phase flow pattern map for evaporation in horizontal tubes: latest version, in: Proceedings of the 1st International Conference on Heat Transfer, Fluid Mechanics and Thermodynamics, Kruger Park, South Africa, vol. 1, 2002, pp. 182–188.

[22] J.G. Collier, J.R. Thome, Convective Boiling and Condensation, third ed., Oxford University Press, Oxford, 1994.

[23] O. Zürcher, J.R. Thome, D. Favrat, Evaporation of ammonia in a smooth horizontal tube: heat transfer measurements and predictions, J. Heat Transfer 121 (1999) 89–101.

[24] H.M. Soliman, On the annular-to-wavy flow pattern transition during condensation inside horizontal tubes, Can. J. Chem. Eng. 60 (1982) 475–481.